High-Performance $NaK_2Li[Li_3SiO_4]_4$:Eu Green Phosphor for Backlighting Light-Emitting Diodes

High-Performance $NaK_2Li[Li_3SiO_4]_4$:Eu Green Phosphor for Backlighting Light-Emitting Diodes

Mu-Huai Fang,[†,#] Carl Osby M. Mariano,[§,#] Kuan-Chun Chen,[†] Jia-Cheng Lin,[†] Zhen Bao,[†] Sebastian Mahlik,[Φ,Ψ] Tadeusz Lesniewski,[Φ] Kuang-Mao Lu,[£] Ying-Rui Lu,[Ω] Yu-Jong Wu,[Ω] Hwo-Shuenn Sheu,[Ω] Jyh-Fu Lee,[Ω] Shu-Fen Hu,[§,*] Ru-Shi Liu[†,*], and J. Paul Attfield[¥,*]

[†]Department of Chemistry, National Taiwan University, Taipei 106, Taiwan

[§]Department of Physics, National Taiwan Normal University, Taipei 116, Taiwan

[Φ]Institute of Experimental Physics, Faculty of Mathematic, Physics and Informatics, Gdańsk University, Wita Stwosza 57, 80-308 Gdańsk, Poland

[Ψ]Graduate School of Human and Environmental Studies, Kyoto University, Kyoto 606-8501, Japan

[£]Everlight Electronics Co., Ltd., New Taipei City 238, Taiwan

[Ω]National Synchrotron Radiation Research Center, Hsinchu 300, Taiwan

[¥]Centre for Science at Extreme Conditions and School of Chemistry, University of Edinburgh, King's Buildings, Mayfield Road, EH9 3JZ Edinburgh, U.K.

ABSTRACT: Narrowband green phosphors with high quantum efficiency are required for backlighting white light-emitting diode (WLED) devices. Materials from the $A[Li_3SiO_4]_4:Eu^{2+}$ family have recently been proposed as having superior properties to industry-standard β-SiAlON green phosphors. Here we show that a cheap, easily synthesized host $NaK_2Li[Li_3SiO_4]_4$ (NKLLSO) doped with a mixture of $Eu^{2+}$and Eu^{3+} is an outstanding narrowband green phosphor, with an external quantum efficiency of 51% and superb thermal stability (97.1% of room temperature performance at 150 °C). Structural studies reveal that green emission occurs from two Eu^{2+}sites, while Eu^{3+} introduces a high concentration of vacancies that may suppress quenching from energy transfer between Eu^{2+} sites. A WLED package constructed using our NKLLSO phosphor shows extremely high color vividness, competitive with a β-SiAlON comparator. This work will stimulate further research on efficient green phosphors for practical WLED devices.

INTRODUCTION

Highly efficient phosphors with narrowband emission and good thermal stability are urgently needed for white backlighting light-emitting diodes (WLEDs).[1] Narrowband emission enhances the color rendition and enlarges the color gamut value, while good thermal stability prevents color distortion over different operating temperatures.[2] Much effort has been put into the development of narrowband red-emitting phosphors, but less attention has been paid to narrowband green phosphors. Low-oxygen β-SiAlON (low-z β-$Si_{6-z}Al_zO_zN_{8-z}$ with $z < 0.2$) is still dominant as a backlighting green phosphor due to its narrow bandwidth (49 nm; 1772 cm^{-1}) and suitable emission wavelength (529 nm) despite a low external quantum efficiency of around 30%.[3] Many UCr_4C_4-type phosphors have been reported in recent years, starting with $SrLiAl_3N_4:Eu^4$ and other nitride or oxy-nitride materials with orange to deep-red emission.[5–13] Eu-doped UCr_4C_4-type oxide phosphors were subsequently developed with narrowband blue-emitting and green-emitting properties,[14–18] but these have not had such high efficiencies. Among all of them, $NaK_2Li[Li_3SiO_4]_4$:Eu attracts our attention, which was first revealed in the patent of WO 2018/029299; however, only basic photoluminescent and structural information was provided.[19] In this study, highly-efficient narrowband UCr_4C_4-type green-emitting $NaK_2Li[Li_3SiO_4]_4$:Eu (NKLLSO) phosphors are synthesized and their photoluminescent and underlying structural properties are characterized, revealing the great potential for WLED backlighting applications.

EXPERIMENTAL METHODS

A solid-state reaction method was applied to synthesize all samples used in this study. The starting precursors for synthesis were Na_2O (Aldrich, 99.8%), K_2CO_3 (Baker, 99.0%), Li_2O (Aldrich, 99.5%), SiO_2 (Aldrich, 99.995%), Eu_2O_3 (Aesar, 99.99%), and H_3BO_3 (Aldrich 99%). The precursors were first weighted stoichiometrically, then mixed and ground on an agate mortar until homogenous. The ground precursors were put into an alumina crucible and subjected to sintering at 750 °C for 4 hours, with a heating and cooling rate of 5 °C/min. Forming gas (10% H_2 + 90% N_2) was used to reduce Eu^{3+} to Eu^{2+}. The samples were then shifted to anhydrous alcohol, and the solution was stirred. We used the pipet to remove the upper part of the solution and then refilled with anhydrous alcohol. This was repeated five times then samples were shifted to a vacuum desiccator. $NaK_2Li[Li_3SiO_4]_4$:Eu was obtained after samples were dried, and only a tiny amount of Li_2SiO_3 impurity exists in the as-prepared samples.

The phosphor-converted light-emitting diodes (pc-LED) was made by mixing with $NaK_2Li[Li_3SiO_4]_4:Eu^{2+}$ phosphor and $K_2SiF_6:Mn^{4+}$ as green and red components for the blue LED (V10J 455–457.5 nm, 23–24.5 mW). Insulation glue (KER3000M2) was utilized to mix $NaK_2Li[Li_3SiO_4]_4:Eu^{2+}$ and $K_2SiF_6:Mn^{4+}$. The green silicate phosphor, β-SiAlON (SW531BH), was chosen as the standard green phosphor with the emission wavelength and bandwidth at 529 and 46 nm, respectively.

Synchrotron X-ray diffraction (SXRD) was performed in the BL01C2 beamline (λ = 0.82657 Å) at the National Synchrotron Radiation Research Center (NSRRC), Taiwan. The data were analyzed by using the Total Pattern Analysis Solutions version 4.2 (TOPAS 4.2). The ratio of Eu^{2+}/Eu^{3+} was examined by Eu L_3-edge of X-ray absorption near-edge structure spectroscopy in fluores-

cence mode at the BL17 beamline in NSRRC, Taiwan. The Eu L_3-edge and K *K*-edge of extended X-ray absorption fine structure experiments were conducted at the BL16A1 beamline in NSRRC, Taiwan.

Photoluminescence excitation and photoluminescence spectra were characterized using a Fluoromax 4P spectrofluorometer. Steady-state optical spectra were obtained using an SR750 grating spectrometer with an iDus420 CCD detector. The luminescence was excited using a He–Cd laser operating at 442 nm. Time-resolved emission spectroscopy (TRES) was performed using an acquisition system consisting of a grating spectrometer coupled to a streak camera, which resolves the spectrally and temporally luminescence signal of the sample under pulsed excitation. The decay curves of the emission bands are obtained by integrating the streak image over wavelength in the desired spectral windows. The excitation light source was a picosecond Nd–YAG laser operating at 355 nm pumping an optical parametric generator (OPG), providing tunable excitation in the spectral range of 230–2000 nm. The low temperature was achieved using a DE204SL closed-cycle helium cryostat. The vacuum ultraviolet excitation and emission spectra were measured at BL03A1 beamline in NSRRC, Taiwan. Quantum yield was acquired using Quantaurus-QY Absolute Photoluminescence Quantum Yield Spectrometer, Hamamatsu, with an excitation source of 450 nm. Temperature-dependent photoluminescence (TDPL) was measured using the Fluoromax-4 spectrophotometer (Horiba, Japan) equipped with a heating device (THMS-600). LED packaging was done by using a blue LED (V10J 455–475.5 nm, 23–24.5 mW).

RESULTS and DISCUSSION

Initial studies of the relative photoluminescent intensity for $Na_{1-x}K_2Li[Li_3SiO_4]_4$:*x*Eu with varying Eu concentrations found the optimum chemical composition to have x = 0.13 (Figure S1). Polycrystalline $Na_{0.87}K_2Li[Li_3SiO_4]_4$:0.13Eu (NKLLSO) was synthesized as described in SI. To obtain detailed structural information, the synchrotron X-ray diffraction (XRD) pattern of the NKLLSO phosphor is analyzed by Rietveld refinement, as shown in Figure 1a. The original structure model is based on the patent of WO 2018/029299 and Hoppe et al.[19,20] In the refinement, we further consider the scatterer contribution of Eu ions. Results are shown in Tables S1 and Table S2. The structure (Figure 1b) has Si^{4+} and some of the Li^+ ions coordinated by four O^{2-} ions to form tetrahedra, which define channels containing Na^+, K^+, and remaining Li^+ ions. K^+ and Na^+ ions are coordinated with eight O^{2-} ions to form a cuboid coordinated environment, as shown in Figure 1c and Figure 1d, while Li^+ in the channel is coordinated by four O^{2-} in a square plane. According to the ionic radii for 8-coordination of K^+ (1.51 Å), Na^+ (1.18 Å), Li^+ (0.59 Å), and Eu^{2+} (1.25 Å), Eu^{2+} may be expected to incorporate into Na^+ and K^+ sites.[21] Interestingly, one can observe some Na^+ deficiency from the refinement results ($Na_{0.76}Eu_{0.12}$) compared to the theoretical value ($Na_{0.87}Eu_{0.13}$). The inductively coupled plasma optical emission spectrometry results also prove this observation (Table S3), which will be discussed in detail in the following content.

The photoluminescence (PL) spectrum, as shown in Figure 2a, consists of a broadband emission with the peak maximum at 528 nm, which is assigned as transitions from the lowest $4f^65d^1$

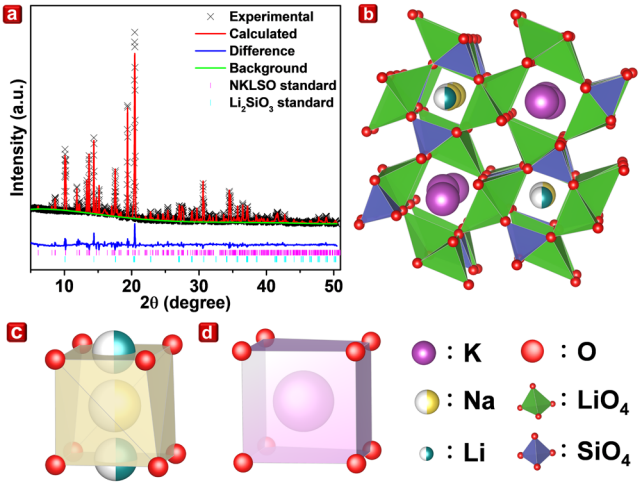

Figure 1. Crystal structure of $Na_{0.87}K_2Li[Li_3SiO_4]_4$:0.13Eu phosphor. (a) Rietveld fit to room temperature powder X-ray diffraction data and (b) crystal structure of the $Na_{0.87}K_2Li[Li_3SiO_4]_4$:0.13Eu phosphor. Local coordination environment of (c) Li^+ and Na^+ ions and (d) K^+ ions.

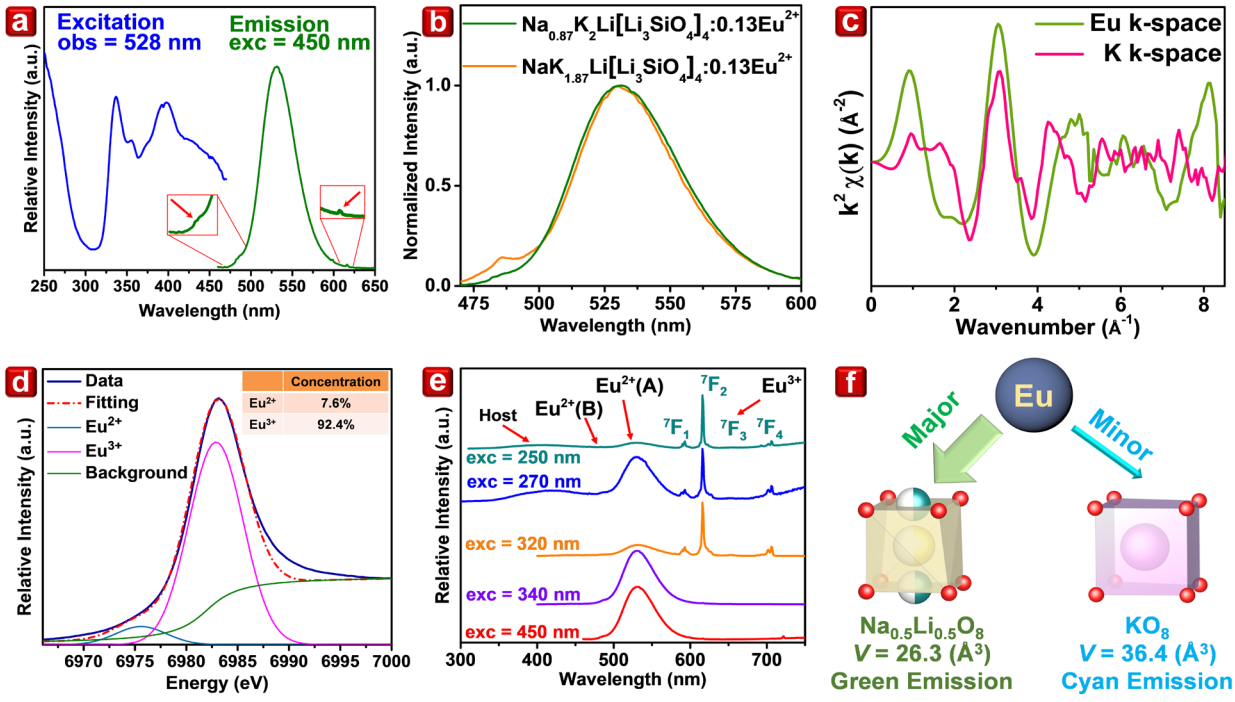

Figure 2. Luminescent properties and local structure of $Na_{0.87}K_2Li[Li_3SiO_4]_4$:0.13Eu. (a) Basic PL and PLE, (b) PL with different Eu-substituted sites, (c) K *K-edge* and Eu L_3-*edge* k^2-weighted Fourier transform of EXAFS spectra, (d) Eu L_3-edge XANES spectrum, and (e) PL at the different excitation wavelengths of $Na_{0.87}K_2Li[Li_3SiO_4]_4$:0.13Eu. (f) Proposed Eu substitution mechanism.

state to the ground state $4f^7$ ($^8S_{7/2}$) of Eu^{2+} ions. The PL excitation (PLE) spectrum monitored at 528 nm consists of several overlapping bands between 320 and 470 nm, which are assigned to the transitions from the ground state $4f^7$ ($^8S_{7/2}$) to the excited states $4f^65d^1$ (^7F_J) of the Eu^{2+} ion. Additionally, an excitation band in the UV region located at wavelengths shorter than 290 nm can also be observed and is attributed to the transition to higher-lying excited states of $4f^65d^1$ configuration of Eu^{2+} ions overlapped with the host absorption. The quantum efficiency of the phosphor materials is a critical issue for practical applications. The internal quantum efficiency (IQE) and external quantum efficiency (EQE) of NKLLSO are up to 81% and 51%, respectively, which reveals great potential in backlighting systems (Table S4).

NKLLSO displays two unusual PL spectral features, as shown in the inset figure in Figure 2a. The first is a shoulder cyan emission band at around 486 nm. Following a previous study on the litho-orthosilicate phosphors, Eu^{2+} will provide green and cyan (blue) color emission when the cuboid size of EuO_8 is within 26–27 and 29–34 $Å^3$, respectively.[22] The cuboid size of NaO_8 is 26.3 $Å^3$ in NKLLSO, leading to a strong green emission at 528 nm while the cuboid size of KO_8 is 36.4 $Å^3$, which is a little out of the cyan emission range. However, local structural relaxation is expected to reduce the cuboid size of K^+ sites occupied by Eu^{2+} due to their size mismatch. It is expected to decrease cyan emission, as shown in Figure 2f. To further elucidate the preferred site occupancy, the PL spectra of synthesized $Na_{0.87}K_2Li[Li_3SiO_4]_4$:0.13Eu and $NaK_{1.87}Li[Li_3SiO_4]_4$:0.13Eu were examined, as shown in Figure 2b. A stronger cyan emission is observed from $NaK_{1.87}Li[Li_3SiO_4]_4$:0.13Eu, consistent with a greater occupancy of K^+ sites by Eu^{2+} in this material.

Eu^{2+} dopant sites in the UCr_4C_4 alkali-lithosilicate phosphors have not previously been investigated by extended X-ray absorption fine structure (EXAFS), so a study has been conducted to discover whether Eu occupies the Na^+ or K^+ site in the NKLLSO structure. Although the best solution is to compare the oscillation patterns between Eu, K, and Na, the low absorption edge of Na (~1071 eV) makes it difficult to be measured by the synchrotron X-ray. K *K-edge* and Eu L_3*-edge* k^2-weighted Fourier transform of EXAFS spectra were obtained, as shown in Figure 2c. The oscillation patterns of Eu and K are clearly different, indicating that the Eu ions are not at the K^+ site. The result is in good agreement with the expectation that Eu should be situated at the Na^+ site rather than the K^+ site based on their cuboid size.[22]

To explore the oxidation state of the Eu ions, the Eu L_3-edge X-ray absorption near-edge structure (XANES) spectrum of NKLLSO was examined, as shown in Figure 2d. Signals from Eu^{2+} and Eu^{3+} are located around 6974 and 6984 eV, respectively. Surprisingly, the results indicate that most of the Eu ions in NKLLSO are in the Eu^{3+} state, with only 7.6% of the Eu in the Eu^{2+} state. The presence of Eu^{3+}, which has weak *f-f* forbidden transitions, explains why a sharp-line emission in NKLLSO is observed. At some excitation wavelengths, the Eu^{3+} emission is even greater than that for Eu^{2+}, as shown in Figure 2e. A further weak broadband emission which extends between 340 and 460 nm can be excited by very short wavelengths below 275 nm. This luminescence is probably associated with the host and is probably associated with the self-trapped exciton emission. This is not an emission coming from Eu^{2+} or Eu^{3+} as the luminescence decay time is in the range of tens μs, as shown in Figure S2.

To further understand the luminescent properties from Eu^{2+} and Eu^{3+}, the vacuum ultraviolet (UV) excitation spectra are analyzed using synchrotron radiation, as shown in Figure S3a. When detecting the Eu^{3+} sharp emission at 615 nm, the excitation spectrum has a peak maximum at 217 nm. This peak may be attributed to the charge transfer signal, which measures the energy between the valance band and the Eu^{3+} ground state. On the other hand, there are three excitation peaks at 247, 200, and 170 nm that lead to 528 nm Eu^{2+} emission. The peaks at 247 and 200 nm correspond to *f-d* transitions from the ground state to higher *d* levels in Eu^{2+} (Figure S3b), while the peak at 170 nm may be the interband transition. These results support the discovery from the XANES spectra that a large amount of Eu^{3+} ions are in $NaK_2Li[Li_3SiO_4]_4$:Eu. Compared to the emission spectrum excited at 217 nm, an additional sharp emission peak at 606.5 nm is observed when excited at 170 nm (Figure S3d). Moreover, the excitation spectra detected at 615 and 606.5 nm are quite different (Figure S3c). These results demonstrate that there are at least two Eu^{3+} emission centers.

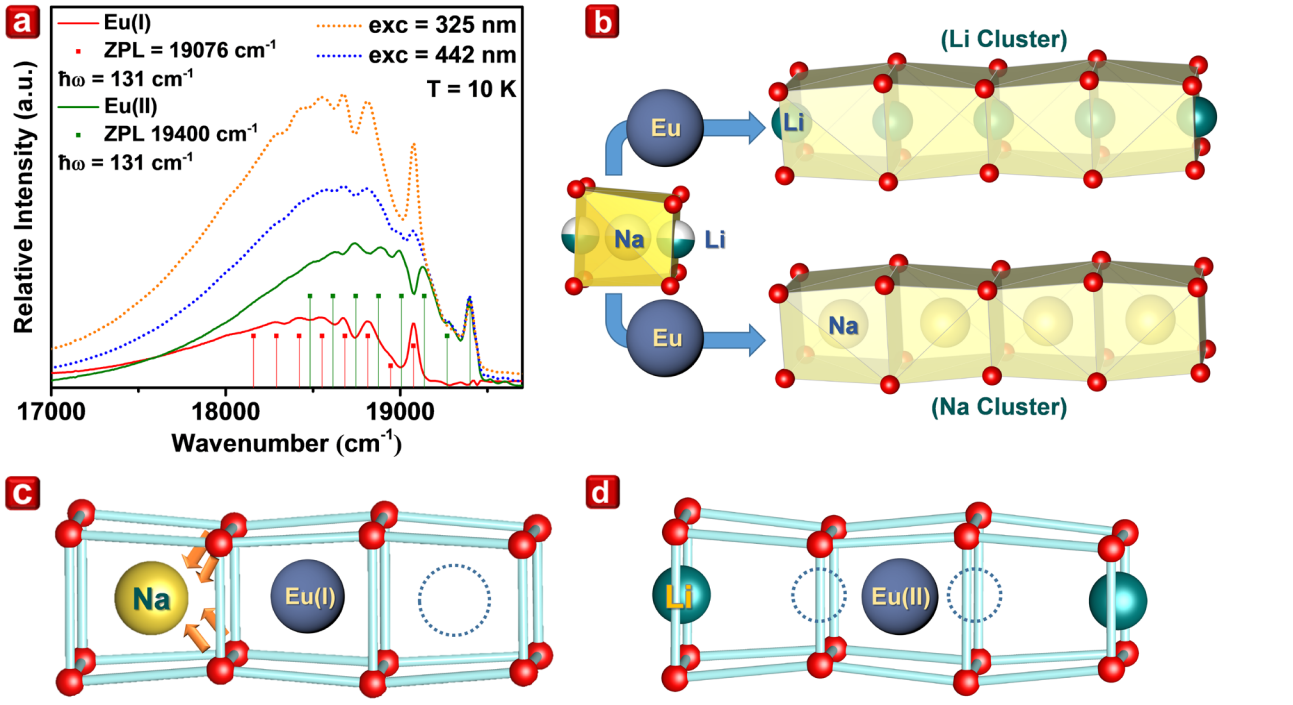

Figure 3. Evidence of alkali metal clustering in the structure and its influence on luminescent properties. (a) Photoluminescence of $Na_{0.87}K_2Li[Li_3SiO_4]_4$:0.13Eu at 10 K with different excitation wavelengths. (b) Clustered coordinated environments of Li^+ and Na^+ in the channel. Schemes of the local coordinated environment of Eu^{2+} in (c) Na^+ cluster, and (d) Li^+ cluster.

Notably, the concentration of Eu^{3+} in NKLLSO is much higher than that of Eu^{2+}, which is unusual in Eu-doped phosphors. This is likely because the loss of Na^+ and Li^+ during the high-temperature synthesis is charge compensated by oxidation of Eu to the Eu^{3+} state.[12] This is also be observed in the UCr_4C_4-type $SrLiAl_3N_4$:Eu phosphor. Although the ratio between Eu^{2+}:Eu^{3+} is low (7.6:92.4 from XANES), the overall Eu molar concentration is 6.5%, which is much higher than in typical phosphor materials. The EQE has been measured with excitation at 450 nm, exciting only Eu^{2+} ions. The high quantum efficiency of up to 51% indicates that Eu^{3+} does not suppress the Eu^{2+} luminescence, and it may even enhance it through suppression of energy transfer between Eu^{2+} ions as described later.

For most phosphors with highly-rigid structures, a clear phonon structure in the PL spectrum is observed when lowering the temperature.[4] Hence, the PL spectra at 10 K with different excitation wavelengths were measured, as shown in Figure 3a. Surprisingly, it turns out that different excitations give slightly different emission spectra, which consist of broadband with a well resolved sharp-lined fine structure. This suggests that two different Eu^{2+} luminescence centers contribute to the green emission spectrum. We focus here only on the green emission from the Eu^{2+} in the Na^+ sites in NKLLSO. If we subtract the spectra, it is possible to decompose the vibrational structure of the emission transition for both Eu^{2+} centers as shown in red and green curves, labeled as Eu(I) and Eu(II), respectively. The zero-phonon line energy for Eu(I) is observed at 19076 cm^{-1} and the phonon energy from the separation of vibrational features is 131 cm^{-1}. For the Eu(II) center, the zero-phonon line energy is observed at 19400 cm^{-1} and the phonon energy is also 131 cm^{-1}. The sites differ mainly in the energy of the zero-phonon line. Similar phenomena were observed in $SrLiAl_3N_4$:Eu, where the structure in the Eu^{2+} emission spectrum was also observed.[23]

It is interesting to notice that phonon repletion intensities were seen in PL (Figure 3a) do not follow the Pekarian relation:[24]

$$I_n = \frac{e^{-S}S^n}{n!} \qquad (1)$$

Where S is the Huang-Rhys factor; n is the n^{th} vibrational levels; I_n is the intensity of the n^{th} vibrational levels. Notably, I_1 is much smaller than I_0 and I_2. Such an effect cannot be interpreted in the framework of a single configurational coordinate diagram where electrons in the lowest state of the $4f^6$ configuration are coupled to the lattice by the symmetrical local mode A_1. The excited state may interact with a two-dimensional lattice model of ϵ symmetry as the lowest component of the excited state, $4f^6 5d$(E), has E symmetry in cuboid-coordinated symmetry so an $Ex\epsilon$ type Jahn-Teller effect is expected. Hence the ground state is not coupled to the lattice.

The configurational coordinate diagram, showing the cross-section on the Q_ϵ axis is presented in Figure S4a. It is seen that the emitting state is characterized by the symmetrical even-parity phonon wave function. The transition that yields the zero-phonon line is also to the symmetrical vibrational wave function. The first phonon repetition in the luminescence spectrum is the transition from the even to odd parity function. As a result, the overlap integral is strongly diminished. The diagram presented in Figure S4a also describes the low-temperature luminescence spectrum from the Eu(I) and Eu(II) sites. To demonstrate that there are two Eu^{2+} luminescence centers, we have measured decay profiles of individual lines by time-resolved spectroscopy and calculated decay times, as shown in Figure S4b. However, only the zero-phonon line of the Eu(II) centers can be separated, which equals 0.86 µs. The rest of the lines overlap, so obtaining their decay times is very difficult. The results indicate that the decay times for each emission wavelength are slightly different and change in the range from 0.88 to 0.90 µs. Taking into account that the decay time of Eu(II) is shorter (0.86 µs), we can estimate that the decay time Eu(I) is around 0.9 µs.

A critical question that remains is why two Eu emission centers are observed when there is only one Na site in the NKLLSO structure? This requires a deeper analysis of the NKLLSO structure. In the Na/Li channels, both the occupancies for Na^+ and Li^+ equal to 0.5 on the average. Moreover, the structural information from X-ray diffraction reveals that the distance from the Li^+ and Na^+ in the channel is only 1.57 Å, which is unrealistically short. Li^+ and Na^+ will likely tend to form short-range clusters, as shown in Figure 3b. This gives rise to two likely Eu^{2+} environments.

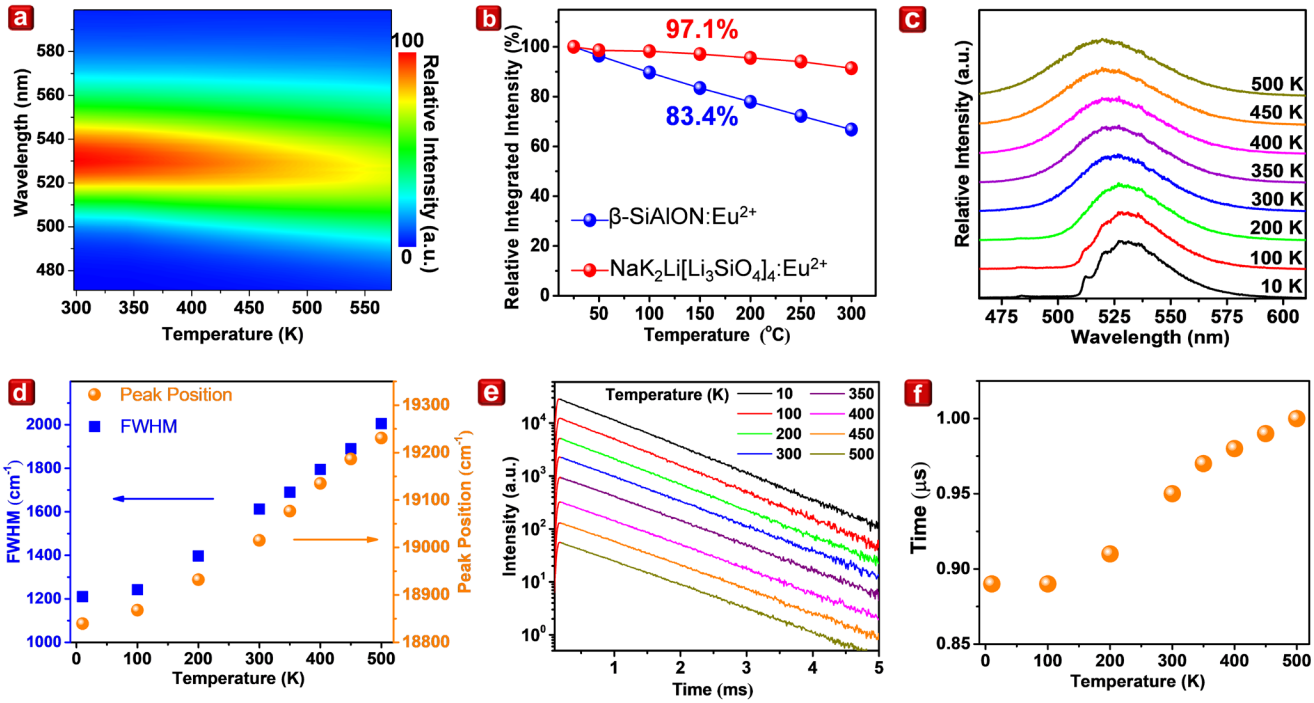

Figure 4. Thermal properties of $Na_{0.87}K_2Li[Li_3SiO_4]_4$:0.13Eu. (a) Contour plot, (b) relative integrated intensity, (c) low-temperature, (d) full width at half maximum of emission band and peak position of the PL peak maximum, (e) temperature-dependent decay curve monitored at 520–550 nm, and (f) decay time of the temperature-dependent photoluminescence of $Na_{0.87}K_2Li[Li_3SiO_4]_4$:0.13Eu.

Eu^{2+} can directly substitute one Na^+ ion, and a nearby Na^+ is removed to balance the change (Figure 3c). Alternatively, Eu^{2+} can incorporate between two Li^+ ion vacancies (Figure 3d). The analysis of the low-temperature PL spectra (Figure 3a), shows that the phonon energy for these two environments is the same as the EuO_8 coordinated sites are quite similar. In the case of Eu^{2+} in the Li^+ cluster (Figure 3d), Li^+ vacancies exist on both sides of Eu^{2+}. In comparison, in the cases of Eu^{2+} in the Na^+ cluster (Figure 3c), a vacancy on one side and a Na^+ on the other can be expected, leading to the distortion of the local environment and increase the crystal field strength. As a result, stronger crystal field strength and slightly red-shift photoluminescence can be expected in the cases of Eu^{2+} in the Na^+ cluster.

Energy transfer between two activators is the key issue that reduces the quantum efficiency, which is related to the distance between the activators. This process will more likely happen if two activators, either Eu^{3+}/Eu^{2+} or Eu^{2+}/Eu^{2+}, are too close. An important consequence of the discovery that much of the Eu is in the Eu^{3+} state is that the Na/K/Li cation vacancy concentration (V) is large, according to the composition $Eu^{2+}_{0.01}Eu^{3+}_{0.12}(Na_{0.87}K_2Li)_{0.935}V_{0.25}[Li_3SiO_4]_4$ determined for NKLLSO following the XANES analysis. Quenching due to energy transfer between Eu^{2+} ions is already small because of their low concentration and hence large separations within the lattice and may be further suppressed by the presence of ~25 cation vacancies for every activator site. By contrast, materials like $SrLiAl_3N_4:Eu^{2+}$ phosphor, when Eu^{2+} is substituted in the Sr position, have no vacancies generated. The presence of low Eu^{2+} and high vacancy concentrations explains the high quantum efficiency of Eu^{2+} in NKLLSO.

To explore the thermal stability, a contour plot of the temperature-dependent photoluminescence (TDPL) spectra of NKLLSO is shown in Figure 4a. This demonstrates that NKLLSO possesses good thermal stability with a little band broadening. To quantitatively evaluate the thermal properties for practical applications, the temperature-dependent integrated peak intensities of low-oxygen β-SiAlON and NKLLSO are compared, as shown in Figure 4b. Low-oxygen β-SiAlON maintains 83.4% of its room-temperature emission intensity at 150 °C, while NKLLSO maintains 97.1% at 150 °C, as shown in Figure 4b. Temperatures of backlighting systems can reach 150 ºC so these results reveal the great potential for practical applications in backlighting.

To explore phonon structure and decay properties, the TDPL spectra of $NaK_2Li[Li_3SiO_4]_4:Eu^{2+}$ at low temperature upon excitation at 325 nm are measured, as shown in Figure 4c. At 10 K, the PL spectrum of $NaK_2Li[Li_3SiO_4]_4:Eu^{2+}$ consists of broadband with vibrational structures. When temperature increases, the vibrational structure gradually decreases and is no longer visible above 100 K. Additionally, typical thermal broadening and blue-shift of the emission band with increasing temperature is observed, as shown in Figure 4d. The luminescence decay curves at different temperatures obtained at a maximum of the luminescence band are also checked, as shown in Figure 4e. By fitting a single exponential decay function to experimental curves, temperature-dependent decay times can be obtained, as shown in Figure 4f. The decay

time slightly increases with the temperature between 10 and 500 K. This finding can be explained as the only spin-allowed transition from the lowest *df* state occurs at low temperatures and hence the probability of transition from this state to the ground state $^8S_{7/2}$ (spin S = 7/2 of the $4f^7$ configuration) is the highest. When the temperature increases, both the lowest *df* state and the higher excited states with S = 5/2 (opposite spin of *d* electron) are occupied. Due to the forbidden transition of these states, the decay time from the average time of all radiative transitions is prolonged at high temperatures.

To evaluate the potential of NKLLSO for practical applications, experiments on LED packages have been conducted. The 450 nm blue LED was utilized as the emitting source, and the phosphor, $K_2SiF_6:Mn^{4+}$ (KSF) was chosen as the red component of the backlighting device due to its narrowband emission and extremely high luminescent intensity. For the green part, the commercial low-oxygen β-SiAlON:Eu^{2+} phosphor is compared against the NKLLSO phosphor. The overall luminescent spectrum, the coverage area in the Commission Internationale de l'clairage (CIE) 1931 color spaces, and other information for the LED devices were calculated, as shown in Figure 5a–c. In the CIE diagram, the chromaticity coordinates of the device using NKLLSO and low-z β-SiAlON:Eu^{2+} are (0.264,0.250) and (0.263,0.251), which are nearly the same. Moreover, the generated area in the CIE diagram by the device using NKLLSO and β-SiAlON:Eu^{2+} (529 nm) is 101.2% and 101.1% of NTSC, revealing extremely high color vividness. The overall brightness of the LED using NKLLSO is also nearly the same as the commercial β-SiAlON:Eu^{2+} (529 nm) narrowband green phosphors. Hence, given the opportunities to further fine-tune NKLLSO through variations of chemical composition, synthesis conditions, or post-synthetic treatment to achieve even better performance, these results reveal the great potential for NKLLSO as the practical green narrowband phosphor in future backlighting devices.

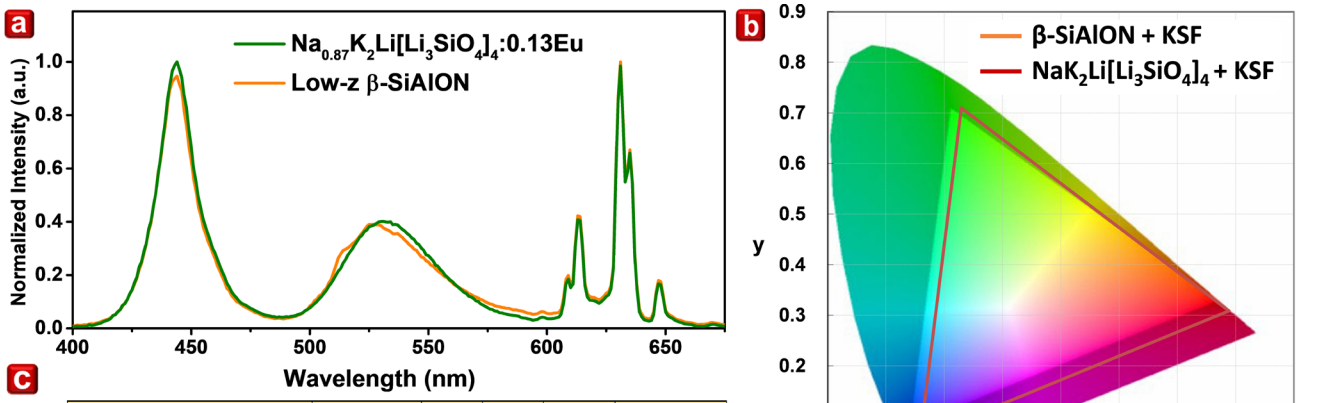

Phosphor		NTSC (CIE-1931)	CIE-x	CIE-y	Φv (lm)	Relative Efficiency
Green	Red					
β-SiAlON (529 nm)	KSF	101.2%	0.264	0.256	47.872	100%
$NaK_2Li[Li_3SiO_4]_4:Eu$	KSF	101.1%	0.262	0.257	47.127	98.4%

Figure 5. Potential for the practical application by the LED package. The 450 nm blue LED chip and the $K_2SiF_6:Mn^{4+}$ red phosphor are used to fabricate the device. β-SiAlON (529 nm) and $Na_{0.87}K_2Li[Li_3SiO_4]_4$:0.13Eu are used as the green component. (a) Luminescent spectrum. (b) Covering area in the Commission Internationale de l'clairage (CIE) 1931 color spaces. (c) Detailed information of the LED device.

CONCLUSIONS

The novel narrowband emission phosphor, $NaK_2Li[Li_3SiO_4]_4$:Eu, synthesized via solid-state reaction, possesses a peak maximum and bandwidth of 528 and 44 nm (1569 cm^{-1}). The exceptionally high external quantum efficiency (51%) is obtained, although only 7.6% of the Eu is in the Eu^{2+} state. This is attributed to the combination of a high average distance between Eu^{2+} activators, with energy transfer quenching further suppressed by a high concentration of cation vacancies. The cuboid coordination process reveals that Eu is preferred to incorporate into the Na^+ site than the K^+ site. As a result, green-emitting and cyan-emitting peaks are assigned to the Eu at Na^+ and K^+ sites, respectively. An extremely high concentration of Eu^{3+} is characterized by XANES and luminescent spectra. Low-temperature PL spectra distinguish two subtly different emission centers for the green-emitting band. These are attributed to local Na-cluster and Li-cluster environments in the channel structure. $NaK_2Li[Li_3SiO_4]_4$:Eu also has excellent thermal quenching properties, with 97.1% of room temperature emission intensity at 150 °C. An LED package using $NaK_2Li[Li_3SiO_4]_4$:Eu and K_2SiF_6:Mn^{4+} as the green and red phosphors can cover 101.1% in NTSC, revealing a great future potential in backlighting devices. This study reveals an outstanding novel narrowband green phosphor and also demonstrates how local structure and defects tune the luminescent centers.

■ ASSOCIATED CONTENT

Supporting Information

Synchrotron refinement results, ICP analysis, and PL excitation and emission results supplied as Supporting Information. Supporting Information is available free of charge via the Internet at http://pubs.acs.org.

■ AUTHOR INFORMATION

Corresponding Authors

sfhu.hu@gmail.com
rsliu@ntu.edu.tw
j.p.attfield@ed.ac.uk

Notes

The authors declare no competing financial interest.

[#]Mu-Huai Fang and Carl Osby M. Mariano contributed equally to this paper.

■ ACKNOWLEDGMENTS

This work was supported by the Ministry of Science and Technology of Taiwan (Contract Nos. MOST 109-2112-M-003-011, MOST 109-2113-M-002-020-MY3, MOST 107-2113-M-002-008-MY3, MOST 110-2923-M-002-017-MY3, MOST 107-2923-M-002-004-MY3, and MOST 106-2112-M-003-007-MY3), the National Science Centre Poland Grant Opus (No. 2016/23/B/ST3/03911 and No. 2019/33/B/ST3/00406, and The National Centre for Research and Development Poland Grant (No. PL-TW/V/1/2018). J.P.A. acknowledges financial support from EPSRC, U.K.

■ References

(1) Fang, M. H.; Leaño, J. L.; Liu, R. S. Control of Narrow-Band Emission in the Phosphor Materials for the Application in Light-Emitting Diodes. *ACS Energy Lett.* **2018**, *3*, 2573–2586.

(2) Fang, M. H.; Yang, T. H.; Lesniewski, T.; Lee, C.; Mahlik, S.; Grinberg, M.; Peterson, V. K.; Didier, C.; Pang, W. K.; Su, C.; Liu, R. S. Hydrogen-Containing $Na_3HTi_{1-x}Mn_xF_8$ Narrow-Band Phosphor for Light-Emitting Diodes. *ACS Energy Lett.* **2019**, *4*, 527–533.

(3) Zhang, X.; Fang, M. H.; Tsai, Y. T.; Lazarowska, A.; Mahlik, S.; Lesniewski, T.; Grinberg, M.; Pang, W. K.; Pan, F.; Liang, C.; Liu, R. S. Controlling of Structural Ordering and Rigidity of β-SiAlON:Eu through Chemical Cosubstitution to Approach Narrow-Band-Emission for Light-Emitting Diodes Application. *Chem. Mater.* **2017**, *29*, 6781–6792.

(4) Pust, P.; Weiler, V.; Hecht, C.; Tücks, A.; Wochnik, A. S.; Henß, A.-K.; Wiechert, D.; Scheu, C.; Schmidt, P. J.; Schnick, W. Narrow-Band Red-Emitting $Sr[LiAl_3N_4]$:Eu^{2+} as a Next-Generation LED-Phosphor Material. *Nat. Mater.* **2014**, *13*, 891–896.

(5) Pust, P.; Hintze, F.; Hecht, C.; Weiler, V.; Locher, A.; Zitnanska, D.; Harm, S.; Wiechert, D.; Schmidt, P. J.; Schnick, W. Group (III) Nitrides $M[Mg_2Al_2N_4]$(M= Ca, Sr, Ba, Eu) and $Ba[Mg_2Ga_2N_4]$ Structural Relation and Nontypical Luminescence Properties of Eu^{2+} Doped Samples. *Chem. Mater.* **2014**, *26*, 6113–6119.

(6) Fang, M. H.; Mahlik, S.; Lazarowska, A.; Grinberg, M.; Molokeev, M. S.; Sheu, H. S.; Lee, J. F.; Liu, R. S. Structural Evolution and Neighbor-Cation Control of Photoluminescence in $Sr(LiAl_3)_{1-x}(SiMg_3)_xN_4$:$Eu^{2+}$ Phosphor. *Angew. Chem. Int. Ed.* **2019**, *58*, 7767–7772.

(7) Schmiechen, S.; Schneider, H.; Wagatha, P.; Hecht, C.; Schmidt, P. J.; Schnick, W. Toward New Phosphors for Application in Illumination-Grade White Pc-LEDs: The Nitridomagnesosilicates $Ca[Mg_3SiN_4]$:Ce^{3+}, $Sr[Mg_3SiN_4]$:Eu^{2+}, and $Eu[Mg_3SiN_4]$. *Chem. Mater.* **2014**, *26*, 2712–2719.

(8) Fang, M. H.; Meng, S. Y.; Majewska, N.; Lesniewski, T.; Mahlik, S.; Grinberg, M.; Sheu, H.-S.; Liu, R. S. Chemical Control of $SrLi(Al_{1-x}Ga_x)_3N_4$:Eu^{2+} Red Phosphor at Extreme Condition for the Application in Light-Emitting Diodes. *Chem. Mater.* **2019**, *31*, 4614–4618.

(9) Hu, W. W.; Ji, W. W.; Khan, S. A.; Hao, L. Y.; Xu, X.; Yin, L. J.; Agathopoulos, S. Preparation of $Sr_{1-x}Ca_xLiAl_3N_4$:Eu^{2+} Solid Solutions and Their Photoluminescence Properties. *J. Am. Ceram. Soc.* **2016**, *99*, 3273–3279.

(10) Wagatha, P.; Weiler, V.; Schmidt, P. J.; Schnick, W. Tailoring Emission Characteristics: Narrow-Band Red Luminescence from SLA to $CaBa[Li_2Al_6N_8]$:Eu^{2+}. *Chem. Mater.* **2018**, *30*, 7885–7891.

(11) Hoerder, G. J.; Seibald, M.; Baumann, D.; Schröder, T.; Peschke, S.; Schmid, P. C.; Tyborski, T.; Pust, P.; Stoll, I.; Bergler, M.; Patzig, C.; Reißaus, S.; Krause, M.; Berthold, L.; Höche, T.; Johrendt, D.; Huppertz, H. $Sr[Li_2Al_2O_2N_2]$:Eu^{2+}—A High Performance Red Phosphor to Brighten the Future. *Nat. Commun.* **2019**, *10*, 1824.

(12) Fang, M. H.; Tsai, Y.-T.; Sheu, H.-S.; Lee, J.-F.; Liu, R. S. Pressure-Controlled Synthesis of High-Performance $SrLiAl_3N_4$:Eu^{2+} Narrow-Band Red Phosphors. *J. Mater. Chem. C* **2018**, *6*, 10174–10178.

(13) Hoerder, G. J.; Peschke, S.; Wurst, K.; Seibald, M.; Baumann, D.; Stoll, I.; Huppertz, H. $SrAl_{2-x}Li_{2+x}O_{2+2x}N_{2-2x}$:$Eu^{2+}$ ($0.12 \leq x \leq 0.66$)—Tunable Luminescence in an Oxonitride Phosphor. *Inorg. Chem.* **2019**, *58*, 12146–12151.

(14) Zhao, M.; Zhou, Y.; Molokeev, M. S.; Zhang, Q.; Liu, Q.; Xia, Z. Discovery of New Narrow-Band Phosphors with the UCr_4C_4-Related Type Structure by Alkali Cation Effect. *Adv. Opt. Mater.* **2019**, *7*, 1801631.

(15) Dutzler, D.; Seibald, M.; Baumann, D.; Philipp, F.; Peschke, S.; Huppertz, H. $RbKLi_2[Li_3SiO_4]_4$:Eu^{2+} an Ultra Narrow-Band Phosphor. *Z. Naturforsch. B* **2019**, *74*, 535–546.

(16) Wang, L.; Kong, X.; Li, P.; Ran, W.; Lan, X.; Chen, Q.; Shi, J. Narrow-Band Green Emission of Eu^{2+} in a Rigid Tunnel Structure: Site Occupations, Barycenter Energy Calculations and Luminescence Properties. *Inorg. Chem. Front.* **2019**, *6*, 3604–3612.

(17) Ruegenberg, F.; Seibald, M.; Baumann, D.; Peschke, S.; Schmid, P. C.; Huppertz, H. Novel Double Band Emitter with

Ultra-Narrow Band Blue and Narrow Band Green Luminescence. *Chem. Eur. J.* **2020**, *26*, 1–8.

(18) Wang, W.; Tao, M.; Liu, Y.; Wei, Y.; Xing, G.; Dang, P.; Lin, J.; Li, G. Photoluminescence Control of UCr_4C_4-Typed Phosphors with Superior Luminous Efficiency and High Color Purity via Controlling Site-Selection of Eu^{2+} Activators. *Chem. Mater.* **2019**, *31*, 9200–9210.

(19) Seibald, M.; Baumann, D.; Fiedler, T. I. M.; Lange, S.; Huppertz, H.; Dutzler, D.; Schroeder, T.; Bichler, D.; Plundrich, G.; Peschke, S.; Hoerder, G.; Achrainer, G.; Wurst, K. Luminophore And Process For Producing A Luminophore. Patent WO2018/029299, 2016.

(20) Hofmann, J.; Brandes, R.; Hoppe, R. New Silicates with "Stuffed Pyrgoms": $CsKNaLi_9(Li(SiO_4))_4$ (I), $CsKNa_2Li_8(Li(SiO_4))_4$ (II), $RbNa_3Li_8(Li(SiO_4))_4$ (III) and $RbNaLi_4(Li(SiO_4))_2$ (IV). *Z. Anorg. Allg. Chem.* **1994**, *620*, 1495–1508.

(21) Shannon, R. D. Revised Effective Ionic Radii and Systematic Studies of Interatomic Distances in Halides and Chalcogenides. *Acta Crystallogr.* **1976**, *32*, 751–767.

(22) Fang, M. H.; Mariano, C. O. M.; Chen, P. Y.; Hu, S. F.; Liu, R. S. Cuboid-Size-Controlled Color-Tunable Eu-Doped Alkali-Lithosilicate Phosphors. *Chem. Mater.* **2020**, *32*, 1748–1759.

(23) Tsai, Y. T.; Nguyen, H. D.; Lazarowska, A.; Mahlik, S.; Grinberg, M.; Liu, R. S. Improvement of the Water Resistance of a Narrowband Red-Emitting $SrLiAl_3N_4:Eu^{2+}$ Phosphor Synthesized under High Isostatic Pressure through Coating with an Organosilica Layer. *Angew. Chem. Int. Ed.* **2016**, *55*, 9652–9656.

(24) Di Bartolo, B.; Armagan, G., *Spectroscopy of Solid-State Laser-Type Materials*, Springer Science & Business Media, 2012.

TOC Graphic